Journal of Geoscience and Environment Protection, 2026, 14(6), 98-108
https://www.scirp.org/journal/gep
ISSN Online: 2327-4344
ISSN Print: 2327-4336

Modelling of *In-Situ* Soil Water Characteristics Based on Multiple-Years Monitoring

Ippei Iiyama

School of Agriculture, Utsunomiya University, Utsunomiya, Japan
Email: iiyama@a.utsunomiya-u.ac.jp

How to cite this paper: Iiyama, I. (2026). Modelling of *In-Situ* Soil Water Characteristics Based on Multiple-Years Monitoring. *Journal of Geoscience and Environment Protection, 14,* 98-108.
https://doi.org/10.4236/gep.2026.146006

Received: April 21, 2026
Accepted: June 21, 2026
Published: June 24, 2026

Abstract

Soil water characteristics are one of the essential factors for understanding storage and flow of water in soils, recognized as a series of relations between soil water potential ψ [J·kg^{-1}] and soil water content θ [m^3·m^{-3}]. Because a series of ψ-θ relations shows hysteretic behaviors, it is often difficult to correctly express it by using a single-valued function θ (ψ). Aiming at describing *in-situ* soil water hysteresis, this study formulated a model of soil water hysteresis based on ψ-θ relations observed in a field. The model assumption derived from the observed features was that any scanning curve is a similitude of a corresponding main curve on the ψ-θ plane. The model can work along randomly-ordered drying-wetting cycles by citing only a pair of the main curves. The two main curves should share the driest and wettest extremities, while there is almost no restriction on the types of mathematical functions to express any of the main curves. The model algorithm allows for calculating an unknown water content θ_1 [m^3·m^{-3}] for a given water potential ψ_1 [J·kg^{-1}] by citing a latest known moisture condition (ψ_0, θ_0). The model reproduced well the general trend of the measured ψ-θ relations throughout the study period, except for the cases in which the chances of reversals in drying-wetting directions were wrongly input into the model in the series of measurements of ψ [J·kg^{-1}]. It was also difficult for the model to reproduce a long continual wetting process found in the domain of $\psi \geq -1$ [J·kg^{-1}], implying the possible improvement of the model performance by modifying the model so that the model can deal with multi-modal pore systems like volcanic ash soils or other types of structured soils rich in soil aggregates.

Keywords

Drying and Wetting Cycles, Main Curves, Moisture Characteristics, Scanning Curves, Soil Water Hysteresis, Water Content, Water Potential, Water Retention

1. Introduction

Characteristics of how a soil retains water are represented by a relation between soil water content θ [$m^3 \cdot m^{-3}$] and soil water potential ψ [$J \cdot kg^{-1}$]. And a curve drawn by a series of ψ-θ plots obtained through drying or wetting the soil is called a soil water retention curve (SWRC). A SWRC can be approximated as a mathematical function θ(ψ) and is used to diagnose soil moisture conditions or to analyze water flow in soils. However, a field-observed ψ-θ relation is not necessarily expressed by a single-valued function of θ(ψ) but may be described as a multiple-valued function, depending on the direction of change in ψ [$J \cdot kg^{-1}$]. This is called soil water hysteresis.

In soil water hysteresis, a value of θ [$m^3 \cdot m^{-3}$] in a wetting process of a soil becomes larger than that in a drying process for a given ψ [$J \cdot kg^{-1}$] so that the two processes draw two different paths on a ψ-θ plane. The path of ψ-θ relation that is drawn when a soil with its possible maximum water content θ_{max} [$m^3 \cdot m^{-3}$] is incrementally drained toward its possible driest condition with the water content θ_{min} [$m^3 \cdot m^{-3}$] is called the main drying SWRC $\theta_{md}(\psi)$, and the path for its reverse process is called the main wetting SWRC $\theta_{mw}(\psi)$. Since a soil in a field is generally exposed to intermediate moisture conditions between the two extremities through drying-wetting cycles, paths of ψ-θ relations observed in the field should be drawn between the two main curves on the ψ-θ plane and are called scanning drying SWRCs $\theta_{scd}(\psi)$ or scanning wetting SWRCs $\theta_{scw}(\psi)$.

Possible causes of soil water hysteresis have been listed like the "bottle-neck effect", the "contact-angle effect", the entrapment of air in a wetting soil, and any process through which the pore geometry of a soil may vary as time passes with cycles of wetting and drying (Kutilek & Nielsen, 1994; Hillel, 1998). And although these phenomenological interpretations are quite rational, they are also too microscopic or too detailed to be practically modelled by mathematical expressions. As a result, more macroscopic approaches have been proposed and tested for modelling soil water hysteresis.

The independent domain theory (Poulovassilis, 1962; Philip, 1964; Mualem, 1973; Mualem, 1974) and the dependent domain theory (Mualem & Dagan, 1975; Poulovassilis & El-Ghamry, 1978) are pioneering works about modelling soil water hysteresis. These theories have evolved mechanistically and have been confirmed to reproduce and predict well hysteretic behaviors of ψ-θ relations. However, it is often cumbersome to effectively incorporate them into the algorithm to describe the trajectory of ψ-θ plots for many repetitions of drying-wetting cycles. Thus, instead, the empirical model proposed by Scott et al. (1983) has been widely adopted. The conciseness of this model owes mainly to the feature that it can draw a series of $\theta_{scd}(\psi)$ and $\theta_{scw}(\psi)$ by citing only a pair of $\theta_{md}(\psi)$ and $\theta_{mw}(\psi)$ that are expressed with the same type of mathematical function. Application of the empirical model can certainly improve the accuracy of numerically predicting water flow in soils (Kool & Parker, 1987) with such a positive feature that the model can be easily calibrated with a limited number of parameters (Parker & Lenhard, 1987; Lenhard

et al., 1991).

However, there have been a relatively small number of studies that dealt with features of *in-situ* ψ-θ relations when modelling and simulating hysteretic behaviors in SWRC, presumably because there had been relatively few ψ-θ relations obtained from long-term monitoring in fields in the era of model development about soil water hysteresis. On the other hand, recent studies tend to observe *in-situ* ψ-θ relations for longer periods, increasingly clarifying the features of hysteretic behaviors of *in-situ* ψ-θ relations (Bordoni et al., 2017; Zhang et al., 2022; Iiyama, 2024). Therefore, it seems worth developing a model of soil water hysteresis by referring to features of *in-situ* ψ-θ relations.

This study aimed at modelling soil water hysteresis based on features of field-observed ψ-θ relations. The model was developed so that it can be available if the two main curves $\theta_{md}(\psi)$ and $\theta_{mw}(\psi)$ share the driest and wettest extremities θ_{min} [$m^3 \cdot m^{-3}$] and θ_{max} [$m^3 \cdot m^{-3}$] on the ψ-θ plain while it can work even when $\theta_{md}(\psi)$ and $\theta_{mw}(\psi)$ are expressed in different types of mathematical functions from each other.

2. Materials and Methods

2.1. Model Development

The model of hysteretic behaviors in soil water characteristics was developed based on the features of the *in-situ* ψ-θ relations found in Iiyama (2024). The observed features were that any scanning curve on the ψ-θ plain was a similitude of a corresponding main curve and the ratio of the similitude was determined mainly by the distance in the direction of θ [$m^3 \cdot m^{-3}$] between the scanning curve and the corresponding main curve. Because any scanning curve should be formulated in any domain of ψ [$J \cdot kg^{-1}$] with any region of θ [$m^3 \cdot m^{-3}$], the model development should start from an arbitrary point (ψ_0, θ_0) on the ψ-θ plain.

Suppose that a ψ-θ relation has been at any point (ψ_0, θ_0) on a wetting process $\theta_{scw}(\psi)$:

$$\theta_0 = \theta_{scw}\left(\psi_0\right) \tag{1}$$

Then, assume that:

(a1) the wettest extremity for $\theta_{scw}(\psi)$ is the same as that for $\theta_{mw}(\psi)$:

$$\lim_{\psi \to 0} \theta_{scw}\left(\psi\right) = \lim_{\psi \to 0} \theta_{mw}\left(\psi\right) = \theta_{max}, \tag{2}$$

(a2) the domain and range for $\theta_{scw}(\psi)$ are $\psi \geq \psi_0$ [$J \cdot kg^{-1}$] and $\theta_0 \leq \theta$ [$m^3 \cdot m^{-3}$] $\leq \theta_{max}$, (a3) the specific water capacity of $\theta_{scw}(\psi)$ can be approximated as:

$$\frac{\partial \theta_{scw}}{\partial \psi} = \frac{\theta_{max} - \theta_0}{\theta_{max} - \theta_{mw}\left(\psi_0\right)} \frac{\partial \theta_{mw}}{\partial \psi}. \tag{3}$$

Certainly, the amount of water that the soil with the moisture condition (ψ_0, θ_0) can absorb at its maximum should be $\theta_{max} - \theta_0$ [$m^3 \cdot m^{-3}$], while the amount of water that the soil on the main wetting process with $\psi = \psi_0$ [$J \cdot kg^{-1}$] can absorb at its maximum should be $\theta_{max} - \theta_{mw}(\psi_0)$ [$m^3 \cdot m^{-3}$]. Both the observed features and the

phenomenological interpretations support that $\theta_{scw}(\psi)$ can be formulated as the similitude of $\theta_{mw}(\psi)$ with the similarity ratio of $(\theta_{max} - \theta_0)/(\theta_{max} - \theta_{mw}(\psi_0))$ as shown in Equation (3).

When $\theta_{scw}(\psi)$ satisfies the assumptions (a1) through (a3), the following equation can hold true:

$$\frac{\theta_{max} - \theta_{scw}(\psi)}{\theta_{max} - \theta_{mw}(\psi)} = \frac{\theta_{max} - \theta_0}{\theta_{max} - \theta_{mw}(\psi_0)}. \tag{4}$$

And solving Equation (4) for $\theta_{scw}(\psi)$ gives

$$\theta_{scw}(\psi) = \theta_{max} - \frac{\theta_{max} - \theta_0}{\theta_{max} - \theta_{mw}(\psi_0)}\left(\theta_{max} - \theta_{mw}(\psi)\right) \tag{5}$$

The scanning drying SWRC $\theta_{scd}(\psi)$ can be obtained in the same manner as $\theta_{scw}(\psi)$. The derivation of $\theta_{scd}(\psi)$ is based on the following assumptions:

(a4) the driest extremity for $\theta_{scd}(\psi)$ is the same as that for $\theta_{md}(\psi)$:

$$\lim_{\psi \to -\infty} \theta_{scd}(\psi) = \lim_{\psi \to -\infty} \theta_{md}(\psi) = \theta_{min}, \tag{6}$$

(a5) the domain and range for $\theta_{scd}(\psi)$ are $\psi \le \psi_0$ [J·kg^{-1}] and $\theta_{min} \le \theta$ [m^3·m^{-3}] $\le \theta_0$,

(a6) the specific water capacity of $\theta_{scd}(\psi)$ can be approximated as:

$$\frac{\partial \theta_{scd}}{\partial \psi} = \frac{\theta_0 - \theta_{min}}{\theta_{md}(\psi_0) - \theta_{min}} \frac{\partial \theta_{md}}{\partial \psi} \tag{7}$$

These assumptions and the concept of the similitude between the main and scanning drying curves lead to the following equation:

$$\frac{\theta_{scd}(\psi) - \theta_{min}}{\theta_{md}(\psi) - \theta_{min}} = \frac{\theta_0 - \theta_{min}}{\theta_{md}(\psi_0) - \theta_{min}}. \tag{8}$$

And rearranging Equation (8) gives:

$$\theta_{scd}(\psi) = \theta_{min} + \frac{\theta_0 - \theta_{min}}{\theta_{md}(\psi_0) - \theta_{min}}\left(\theta_{md}(\psi) - \theta_{min}\right) \tag{9}$$

By using Equations (5) and (9), an unknown water content θ_1 [m^3·m^{-3}] for a given water potential ψ_1 [J·kg^{-1}] can be calculated from a latest known moisture condition (ψ_0, θ_0) through the following algorithm:

(i) a latest known moisture condition (ψ_0, θ_0) and a new soil water potential ψ_1 [J·kg^{-1}] is given.

(ii) determine $d\psi_1 = \psi_1 - \psi_0$ [J·kg^{-1}].

(iii) judge if the process from (ψ_0, θ_0) to (ψ_1, θ_1) is a wetting one ($d\psi_1 \ge 0$) or a drying one ($d\psi_1 < 0$), select either of $\theta_{scw}(\psi)$ and $\theta_{scw}(\psi)$, and evaluate θ_1 [m^3·m^{-3}], such as:

(iii-a) when $d\psi_1 \ge 0$, θ_1 [m^3·m^{-3}] is determined by using $\theta_{scw}(\psi)$ of Equation (5)

(iii-b) when $d\psi_1 < 0$, θ_1 [m^3·m^{-3}] is determined by using $\theta_{scd}(\psi)$ of Equation (9).

(iv) update (ψ_0, θ_0) with (ψ_1, θ_1) and return to (i).

This algorithm indicates that θ_1 [m^3·m^{-3}] on any of wetting or drying processes

can be derived from ψ_0 [J·kg^{-1}], ψ_1 [J·kg^{-1}], and θ_0 [m^3·m^{-3}], while it does not require any specific values of (ψ, θ) at which drying-wetting direction changes as reversal points. And if the two main curves share the same pair of the two extreme water contents θ_{min} [m^3·m^{-3}] and θ_{max} [m^3·m^{-3}], the model can be run even when the types of the mathematical functions $\theta_{md}(\psi)$ and $\theta_{mw}(\psi)$ are different from each other (Figure 1).

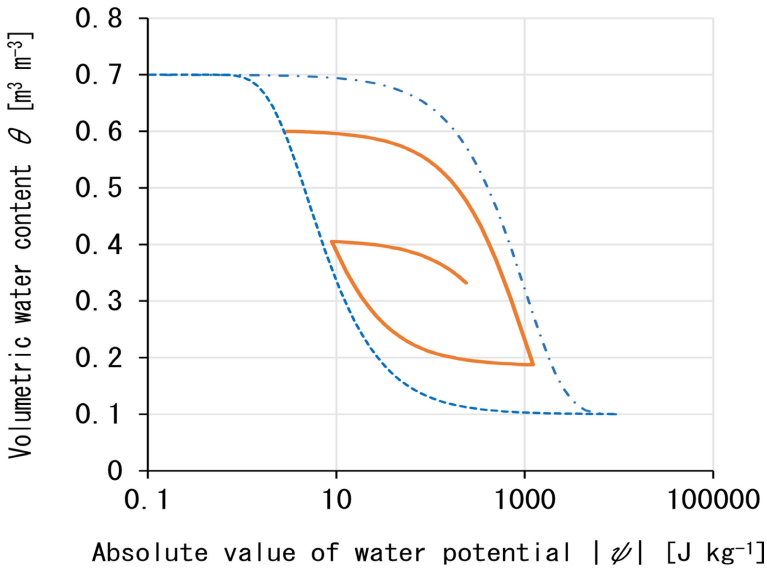

Figure 1. An example of the series of simulated ψ-θ relations obtained by the algorithm (i) through (iv) (solid line). A sample series of ψ was input into the model so that two reversal points are fictitiously given. The main drying and wetting curves used for drawing the scanning curves are expressed as $\theta_{md}(\psi) = \theta_{min} + (\theta_{max} - \theta_{min}) \exp(0.001\psi)$ (dashed line) and $\theta_{mw}(\psi) = \theta_{min} + (\theta_{max} - \theta_{min})(1 - \exp(5/\psi))$ (dotted line), respectively, with $\theta_{min} = 0.1$ [m^3·m^{-3}] and $\theta_{max} = 0.7$ [m^3·m^{-3}]. The types of mathematical function for the main curves are imaginarily selected as a sample pair of main curves.

2.2. Field Data Sets

The model described in the previous section was tuned by using the time series of *in-situ* ψ-θ relations. The *in-situ* data sets were obtained in a meadow field (350 × 80 m; 36˚29'23"N, 139˚59'14"E) located in the Utsunomiya University Farm in Moka city, Tochigi, Japan. The details of the meadow field in this study were described in Iiyama (2024).

Two study sites (sites A and B) were placed at 2 and 8 [m] away from a larch tree row in the study field. And two data-sampling points were set at 0.4 and 1 [m] in depth at each site. The study period was from June 2013 to March 2020. Volumetric water content θ [m^3·m^{-3}] and soil water potential ψ [J·kg^{-1}] had been coincidently measured at each of the sampling points two to three times a week. For measuring θ [m^3·m^{-3}], a capacitance-type soil moisture sensing system (Diviner 2000, Sentek Pty Ltd., Stepney, South Australia) was used. This system was specifically calibrated for the study field (Iiyama, 2016). For measuring ψ [J·kg^{-1}], the tensiometer tubes were permanently installed, and air-pressure in the head space

of each tensiometer tube was measured by a digital manometer (PG-100-102VP; NIDEC COPAL Electronics Corp., Tokyo, Japan), while the height of water column in the tensiometer tube was measured by a tape measure. Then, the measured air-pressure and water column height were converted into a value of ψ [$J \cdot kg^{-1}$].

Among the four sampling points, large and clear hysteretic behaviors on the *in-situ* ψ-θ relations were observed at 1 [m] in depth in the site A (Iiyama, 2024). Thus, this study used the data sets obtained from this sampling point. The soil in this sampling point had the particle density ρ_s of 2.808 [$Mg \cdot m^{-3}$] and the bulk density ρ_d of 0.519 [$Mg \cdot m^{-3}$], indicating that the saturated volumetric water content $\theta_s = 1 - \rho_d/\rho_s$ [$m^3 \cdot m^{-3}$] was 0.815 [$m^3 \cdot m^{-3}$]. And the air-dried water content was 0.050 [$m^3 \cdot m^{-3}$].

2.3. Model Parameters

The model in this study can work when a pair of the main drying and wetting SWRCs $\theta_{md}(\psi)$ and $\theta_{mw}(\psi)$ is given. Thus, it was necessary to select a pair of main SWRCs. Any type of mathematical expression can be taken for describing any of the two main curves, while both main curves should share the water contents at the two extremities θ_{min} [$m^3 \cdot m^{-3}$] and θ_{max} [$m^3 \cdot m^{-3}$]. Thus, among a large number of possibilities about a pair of the two main curves, the following forms were selected in this study:

$$\theta_{md}(\psi) = \theta_{min} + \frac{\theta_{max} - \theta_{min}}{1 + \left|\gamma_d \psi\right|^{\mu_d}} \tag{10}$$

$$\theta_{mw}(\psi) = \theta_{min} + \frac{\theta_{max} - \theta_{min}}{1 + \left|\gamma_w \psi\right|^{\mu_w}} \tag{11}$$

These expressions include six parameters such as γ_d [$kg \cdot J^{-1}$], γ_w [$kg \cdot J^{-1}$], θ_{min} [$m^3 \cdot m^{-3}$], θ_{max} [$m^3 \cdot m^{-3}$], μ_d [$kg \cdot J^{-1}$], and μ_w [$kg \cdot J^{-1}$].

For identifying the parameter set, it was difficult to select a certain subset of the entire measured data set for the parameter identification process, because it had taken most of the study period from June 2013 to March 2020 for the measured ψ-θ relations to complete drawing the largest hysteresis loop on the ψ-θ plane. Therefore, this study hypothesized that if the model developed in this study adequately extracts the features of the *in-situ* ψ-θ relations, at least one parameter set should be found with which the model can explain the hysteretic behaviors of any portions of the measured ψ-θ relations.

Based on the hypothesis, all the measured ψ-θ relations in the study period were used for searching the model parameter set. Then, the simulated ψ-θ relations with the obtained parameter set were compared with the measured ψ-θ relations of each year for the discussion about the performance and weak points of the model in this study.

The parameter values were determined by the method of least squares. The solver add-in of Microsoft Excel was used for minimizing the sum of the squared residuals. Each of the residuals was calculated for each date of measurement as the

difference between the measured and simulated values of θ [$m^3 \cdot m^{-3}$]. The values of the simulated θ [$m^3 \cdot m^{-3}$] were obtained one after another once a known set of θ [$m^3 \cdot m^{-3}$] and ψ [$J \cdot kg^{-1}$] is given as an initial condition, in accord with the recurrence relation described in the model development process.

However, there were 14 times of no measurement period of longer than 1 week among 716 times of measurement in the 82-month study period. Because an occurrence of long no measurement term can disturb the prerequisite of the model that whether an unknown θ_1 [$m^3 \cdot m^{-3}$] will be on a wetting or a drying process depends on its corresponding ψ_1 [$J \cdot kg^{-1}$] and the very latest known pair of ψ_0 [$J \cdot kg^{-1}$] and θ_0 [$m^3 \cdot m^{-3}$]. This means that too long a time period between ψ_0 [$J \cdot kg^{-1}$] and ψ_1 [$J \cdot kg^{-1}$] must prevent the model from judging correct timings and number of reversals in drying-wetting direction during the no measurement period. Thus, every time when a no measurement period occurred, the model running was restarted by setting the pair of ψ [$J \cdot kg^{-1}$] and θ [$m^3 \cdot m^{-3}$] measured just after the no measurement period.

For searching an adequate set of the model parameters, the following conditions were considered from the phenomenological view point:

(c1) $\theta_{max} \leq 0.815$ [$m^3 \cdot m^{-3}$], since the saturated volumetric water content of the soil was 0.815 [$m^3 \cdot m^{-3}$].

(c2) $\theta_{min} \geq 0.050$ [$m^3 \cdot m^{-3}$], since the air-dried water content of the soil was 0.050 [$m^3 \cdot m^{-3}$].

(c3) $\theta_{md}(\psi) \geq \theta_{mw}(\psi)$ for any ψ [$J \cdot kg^{-1}$] in the domain of interest.

(c4) $\theta_{md}(\psi) - \theta_{mw}(\psi) \leq \delta$ for $\psi = -0.01$ [$J \cdot kg^{-1}$], where δ [$m^3 \cdot m^{-3}$] was set as small as possible to make $\theta_{md}(\psi)$ and $\theta_{mw}(\psi)$ asymptotically get close to each other under the almost-saturated condition with $\psi = -0.01$ [$J \cdot kg^{-1}$], equivalent to the soil water suction of about 1 [mmH_2O]. At the same time, when too small a value is assigned to δ [$m^3 \cdot m^{-3}$], the main loop becomes too small to enclose all the measured ψ-θ plots.

3. Results and Discussion

Figure 2 shows the main and scanning curves by the model plotted with the measured ψ-θ relations. The parameter values obtained for Equations (10) and (11) were $\gamma_d = 0.006$ [$kg \cdot J^{-1}$], $\gamma_w = 39.15$ [$kg \cdot J^{-1}$], $\theta_{min} = 0.353$ [$m^3 \cdot m^{-3}$], $\theta_{max} = 0.636$ [$m^3 \cdot m^{-3}$], $\mu_d = 1.146$ [$kg \cdot J^{-1}$], and $\mu_w = 0.647$ [$kg \cdot J^{-1}$], and enabled the resultant two main curves to enclose all the measured ψ-θ plots and to satisfy all the conditions (c1) through (c4).

The trajectory of the modeled ψ-θ relations reproduced the general trend of the measured ψ-θ relations throughout the study period (Figure 2(i)). Particularly, the model successfully explained the measured fact that the ψ-θ plots had consistently resided in the region of θ ≥ 0.50 [$m^3 \cdot m^{-3}$] for the first 4 years (Figures 2(ii)-(v)).

Among the subgraphs for the first 4 years, the model showed a sudden unrealistic upward shift in θ [$m^3 \cdot m^{-3}$] from 0.52 to 0.60 [$m^3 \cdot m^{-3}$] with $\psi \fallingdotseq -1.3$ [$J \cdot kg^{-1}$]

(Figure 2(v)). However, this shift was apparent because there was a no measurement term of more than 1 week between the dates of these two measurements, suggesting that the soil had become almost saturated and, then, dried again during the no measurement period and, as a result, the model failed to recognize the actual rising and lowering in ψ [J·kg^{-1}]. Other cases in which no measurement terms deteriorated the model performance were found for the data sets measured in 2013 through 2015. On Figure 2(ii), Figure 2(iii), and Figure 2(iv), the underestimations of θ [m^3·m^{-3}] took place several times in the region of 0.50 [m^3·m^{-3}] ≤ θ ≤ 0.55 [m^3·m^{-3}] with the domain of −100 [J·kg^{-1}] ≤ ψ ≤ −10 [J·kg^{-1}]. In this domain, the more times reversals of drying-wetting direction occur, the more θ [m^3·m^{-3}] lowered in the study site. The model reproduced well this observed feature and, at the same time, can erroneously predict hysteretic behaviors if the chances of reversals in drying-wetting direction are wrongly input into the model among a series of ψ [J·kg^{-1}].

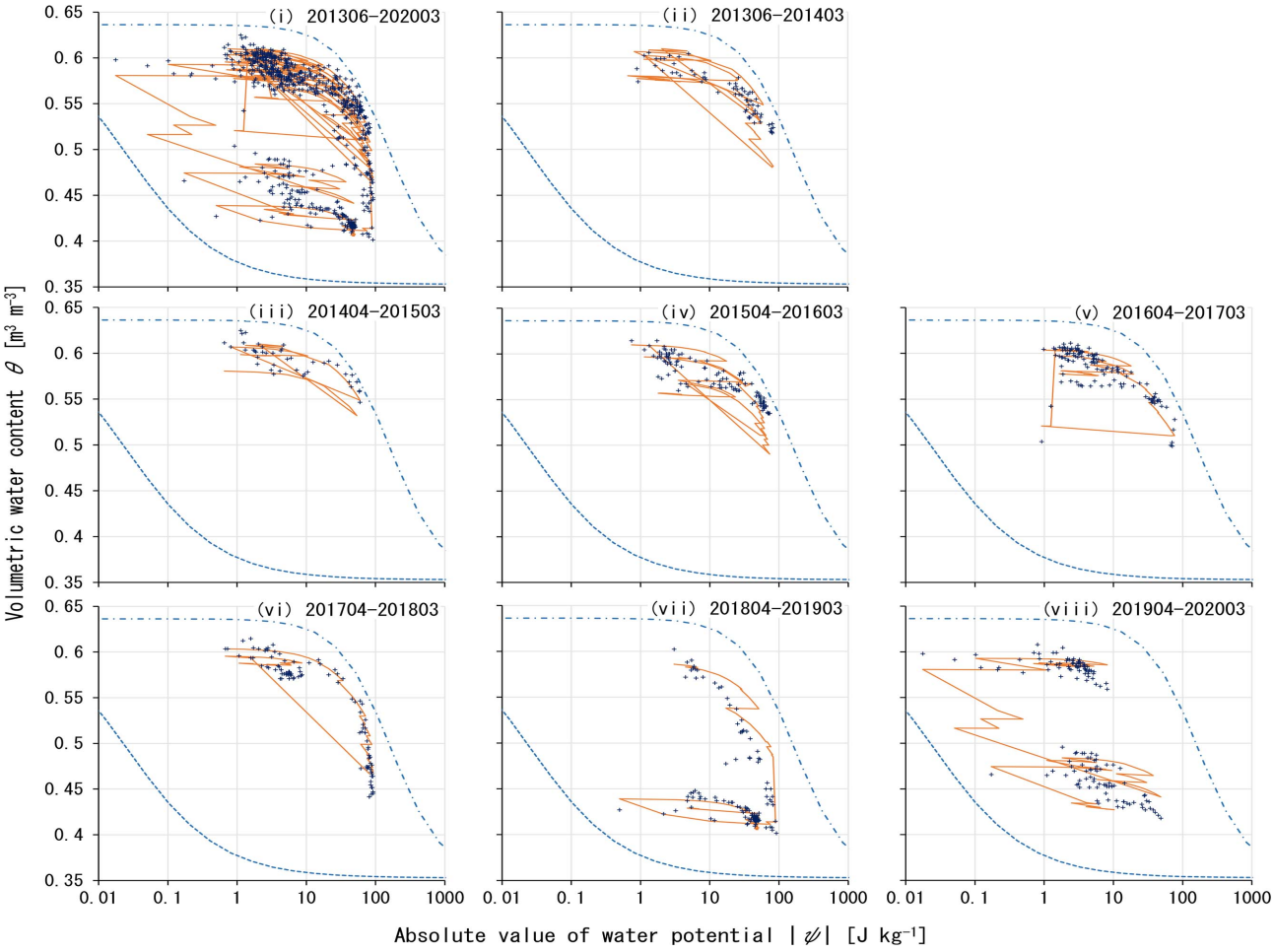

Figure 2. The main curves and scanning curves obtained by fitting the model of soil water hysteresis to the time-series of the measured ψ-θ relations. The dashed and dotted lines in each subgraphs indicate the main drying curve $\theta_{md}(\psi)$ and the main wetting curve $\theta_{mw}(\psi)$, respectively, while the solid line denotes the modeled ψ-θ relations. The measured ψ-θ plots are expressed by the plus symbols "+". The subgraph (i) displays the plots for the entire study period, and each of the subgraphs (ii) through (viii) shows the plots for each year.

The measured θ [$m^3 \cdot m^{-3}$] lowered below 0.50 [$m^3 \cdot m^{-3}$] only in the last 3 years of the study period (**Figures 2(vi)-(viii)**), and the measured ψ [$J \cdot kg^{-1}$] had never gone above −0.1 [$J \cdot kg^{-1}$] except for those in the last year (**Figure 2(viii)**). The model followed well the long continual drying processes found in 2017 and 2018 (**Figure 2(vi)** and **Figure 2(vii)**), while it also reproduced the loop-like behavior of the measured ψ-θ relations in the region of 0.40 [$m^3 \cdot m^{-3}$] ≤ θ ≤ 0.45 [$m^3 \cdot m^{-3}$] with the domain of −100 [$J \cdot kg^{-1}$] ≤ ψ ≤ −0.1 [$J \cdot kg^{-1}$] (**Figure 2(vii)**), suggesting that if the model parameters had been identified without considering the data set measured in the last 3 years, the resultant model would have failed to explain the entire hysteretic behavior observed in the 82 months.

The measured ψ-θ relations traveled from the region of θ ≤ 0.45 [$m^3 \cdot m^{-3}$] to the region of θ ≥ 0.55 [$m^3 \cdot m^{-3}$] in 2019 (**Figure 2(viii)**). This continual wetting process took more than half a year and can be separated roughly into two processes. In the first wetting process, the SWRC shifted up into the region of 0.45 [$m^3 \cdot m^{-3}$] ≤ θ ≤ 0.50 [$m^3 \cdot m^{-3}$] until May in 2019. In the second wetting process, θ [$m^3 \cdot m^{-3}$] became more than 0.55 [$m^3 \cdot m^{-3}$] by October in 2019. The first wetting process was reproduced by the model relatively well. In the second process, on the other hand, the model partially failed to follow the trajectory of the measured ψ-θ relations so that the modeled curve dropped by the region of 0.50 [$m^3 \cdot m^{-3}$] ≤ θ ≤ 0.55 [$m^3 \cdot m^{-3}$] while the measured ψ-θ relations skipped this region and directly reached the region of θ ≥ 0.55 [$m^3 \cdot m^{-3}$].

The failure of the model to reproduce the wetting process in October in 2019 indicated that it was difficult for the model to explain the process in which water is entering into such large pores as filled with water of potential higher than −1 [$J \cdot kg^{-1}$]. This difficulty implied that the model performance can be improved by distinguishing a coarse pore system from the entire pore system of the soil when developing the model of soil water hysteresis.

This study assumed a-priori that the pore size distribution of the soil is of single modal, because single-peaked functions as shown in Equations (10) and (11) were applied to the description of the two main curves. On the other hand, the soil in this study could retain relatively large amount of water in coarse pores and, thus, its *in-situ* SWRC tended to have roughly 10% smaller θ [$m^3 \cdot m^{-3}$] than the corresponding laboratory-measured SWRC under near saturated conditions (Iiyama, 2016). In addition, θ_{max} determined in this study was 0.636 [$m^3 \cdot m^{-3}$], obviously lower than the saturated water content of the soil (0.815 [$m^3 \cdot m^{-3}$]), meaning that the coarse pore system had rarely been filled with water for the study period of 82 months and the resultant measured ψ-θ relations must have prevented the modeling process from correctly considering the drying-wetting cycles of the coarse pore system.

In the same manner as the difference between the determined θ_{max} [$m^3 \cdot m^{-3}$] and the actual saturated water content, θ_{min} determined in this study was 0.353 [$m^3 \cdot m^{-3}$], higher than the air-dried water content of the soil (0.050 [$m^3 \cdot m^{-3}$]). The gap between these two numerals implied that very fine pores in the soil had had almost no experience of drying-wetting cycles, and their soil water characteristics

had no need to be, and were not sufficiently, considered in the model of this study. These features also suggested that it is promising to develop a model that can simulate hysteretic behaviors found in multi-modal pore systems like volcanic ash soils.

4. Conclusion

This study showed the derivation and algorithm of the model of soil water hysteresis that can reproduce the time series of the relations between soil water potential ψ [$J \cdot kg^{-1}$] and soil water content θ [$m^3 \cdot m^{-3}$] along *in-situ* drying-wetting cycles. The assumption of the model derivation was based on the observed features of the *in-situ* ψ-θ relations. The model requires a pair of the main drying and wetting curves $\theta_{md}(\psi)$ and $\theta_{mw}(\psi)$, both of which can be described by any type of mathematical expression only if they share the driest and wettest extremities. The model can calculate an unknown water content θ_1 [$m^3 \cdot m^{-3}$] for a given water potential ψ_1 [$J \cdot kg^{-1}$] and any latest known moisture condition (ψ_0, θ_0), when drawing the series of scanning drying and wetting curves $\theta_{scd}(\psi)$ and $\theta_{scw}(\psi)$.

The model reproduced well the general trend of the measured ψ-θ relations throughout the study period. Particularly, the model imitated the observed processes of ψ-θ relations through which the repetitions of reversals in drying-wetting direction in the domain of $\psi \leq -50$ [$J \cdot kg^{-1}$] caused gradual lowering of θ [$m^3 \cdot m^{-3}$]. However, the model underestimated θ [$m^3 \cdot m^{-3}$] in this domain when the chances of reversals in drying-wetting direction were wrongly input into the model in the series of ψ [$J \cdot kg^{-1}$].

The model also made errors in a long continual wetting process in the domain of $\psi \geq -1$ [$J \cdot kg^{-1}$] in which water entered into coarse pores. This error implied that the model can be improved by separating the whole pore system of the soil into several pore systems including a coarse pore system, as water can hardly enter in and can easily drain from these coarse pores in soils. Therefore, further studies are necessary to modify the model of soil water hysteresis so that it can deal with multi-modal pore systems like volcanic ash soils or other types of structured soils rich in soil aggregates.

Acknowledgements

The author thanks Mr. T. Shiozawa, Mr. E. Saito, Mr. K Seino, and Mr. N. Yamaguchi at the Utsunomiya University Farm who have managed the study field. The author also thanks Mr. T. Hirai of the former student in the Graduate school of Agriculture, Utsunomiya University, and Mr. H. Ajito, Ms. M. Anzai, Ms. K. Arakawa, Ms. M. Cho, Ms. N. Goka, Mr. T. Hoshino, Mr. D. Iimura, Mr. J. Kaneko, Mr. T. Kurata, Mr. K. Ogasawara, Mr. Y. Sakanishi, Mr. H. Shoji, Mr. H. Suto, Mr. S. Takaki, Mr. K. Tezuka, Mr. N. Totsuka, Mr. K. Tsukagoshi, and Mr. Y. Usui of the former students in the Faculty of Agriculture, Utsunomiya University, for their works in the field and in the laboratory.

Conflicts of Interest

The author declares no conflicts of interest regarding the publication of this paper.

References

Bordoni, M., Bittelli, M., Valentino, R., Chersich, S., & Meisina, C. (2017). Improving the Estimation of Complete Field Soil Water Characteristic Curves through Field Monitoring Data. *Journal of Hydrology, 552,* 283-305. https://doi.org/10.1016/j.jhydrol.2017.07.004

Hillel, D. (1998). *Environmental Soil Physics* (pp. 159-161). Academic Press.

Iiyama, I. (2016). Differences between Field-Monitored and Laboratory-Measured Soil Moisture Characteristics. *Soil Science and Plant Nutrition, 62,* 416-422. https://doi.org/10.1080/00380768.2016.1242367

Iiyama, I. (2024). Characteristics of *In-Situ* Soil Water Hysteresis Observed through Multiple-Years Monitoring. *Journal of Geoscience and Environment Protection, 12,* 162-175. https://doi.org/10.4236/gep.2024.125010

Kool, J. B., & Parker, J. C. (1987). Development and Evaluation of Closed-Form Expressions for Hysteretic Soil Hydraulic Properties. *Water Resources Research, 23,* 105-114. https://doi.org/10.1029/wr023i001p00105

Kutilek, M., & Nielsen, D., R. (1994). *Soil Hydrology* (pp. 70-73). Catena Verlag.

Lenhard, R. J., Parker, J. C., & Kaluarachchi, J. J. (1991). Comparing Simulated and Experimental Hysteretic Two-Phase Transient Fluid Flow Phenomena. *Water Resources Research, 27,* 2113-2124. https://doi.org/10.1029/91wr01272

Mualem, Y. (1973). Modified Approach to Capillary Hysteresis Based on a Similarity Hypothesis. *Water Resources Research, 9,* 1324-1331. https://doi.org/10.1029/wr009i005p01324

Mualem, Y. (1974). A Conceptual Model of Hysteresis. *Water Resources Research, 10,* 514-520. https://doi.org/10.1029/wr010i003p00514

Mualem, Y., & Dagan, G. (1975). A Dependent Domain Model of Capillary Hysteresis. *Water Resources Research, 11,* 452-460. https://doi.org/10.1029/wr011i003p00452

Parker, J. C., & Lenhard, R. J. (1987). A Model for Hysteretic Constitutive Relations Governing Multiphase Flow: 1. Saturation-Pressure Relations. *Water Resources Research, 23,* 2187-2196. https://doi.org/10.1029/wr023i012p02187

Philip, J. R. (1964). Similarity Hypothesis for Capillary Hysteresis in Porous Materials. *Journal of Geophysical Research, 69,* 1553-1562. https://doi.org/10.1029/jz069i008p01553

Poulovassilis, A. (1962). Hysteresis of Pore Water, An Application of the Concept of Independent Domains. *Soil Science, 93,* 405-412. https://doi.org/10.1097/00010694-196206000-00007

Poulovassilis, A., & El-Ghamry, W. M. (1978). The Dependent Domain Theory Applied to Scanning Curves of Any Order in Hysteretic Soil Water Relationships. *Soil Science, 126,* 1-8. https://doi.org/10.1097/00010694-197807000-00001

Scott, P., S., Farquhar, G., J., & Kouwen, N. (1983). Hysteretic Effects on Net Infiltration. In American Society of Agricultural Engineers (Ed.), *Advances in Infiltration: Proceedings of the National Conference on Advances in Infiltration* (pp. 163-170). ASAE Publication.

Zhang, P., Chen, G., Wu, J., Wang, C., Zheng, S., Yu, Y. et al. (2022). The Application and Improvement of Soil-Water Characteristic Curves through *in Situ* Monitoring Data in the Plains. *Water, 14,* Article 4012. https://doi.org/10.3390/w14244012